With the possibility of three molecules sharing the shielded area, the expression becomes

$$\theta_{AA3} = \frac{1}{\alpha}\left\{\eta\sigma - \left[\tfrac{1}{2}\,\frac{\eta(\sigma-b)(\sigma-b)}{\alpha(1-\theta_A)}\right]\left[1-\frac{1}{3}\,\frac{\eta(\sigma-b)}{\alpha(1-\theta_A)}\right]\right\} \quad \text{(A3)}$$

In like fashion, when a simultaneous shielding of a portion of the surface by a very large number of molecules is considered, one obtains

$$\theta_{AA} = \frac{\eta\sigma}{\alpha} - \tfrac{1}{2}\left[\frac{\eta(\alpha-b)}{\alpha}\right]^2\frac{1}{1-\theta_A} + \frac{1}{6}\left[\frac{\eta(\sigma-b)}{\alpha}\right]^3\frac{1}{(1-\theta_A)^2} - \frac{1}{24}\left[\frac{\eta(\sigma-b)}{\alpha}\right]^4\frac{1}{(1-\theta_A)^3} + \ldots \quad \text{(A4)}$$

Adding and substracting $\eta b/\alpha$, together with some further manipulation, yields

$$\theta_{AA} = \frac{\eta b}{\alpha} + (1-\theta_A)\left\{\frac{\eta(\sigma-b)}{\alpha(1-\theta_A)} - \frac{1}{2!}\left[\frac{\eta(\sigma-b)}{\alpha(1-\theta_A)}\right]^2 + \frac{1}{3!}\left[\frac{\eta(\sigma-b)}{\alpha(1-\theta_A)}\right]^3 - \frac{1}{4!}\left[\frac{\eta(\sigma-b)}{\alpha(1-\theta_A)}\right]^4 + \ldots\right\} \quad \text{(A5)}$$

Since $\eta b/\alpha = \theta_A$ and $\sigma = 6b$, then $\eta(\sigma - b)/\alpha = 5\theta_A$ and we can write

$$\theta_{AA} = \theta_A + (1-\theta_A)\left[\frac{5\theta_A}{1-\theta_A} - \frac{1}{2!}\left(\frac{5\theta_A}{1-\theta_A}\right)^2 + \frac{1}{3!}\left(\frac{5\theta_A}{1-\theta_A}\right)^3 - \frac{1}{4!}\left(\frac{5\theta_A}{1-\theta_A}\right)^4 + \ldots\right] \quad \text{(A6)}$$

or

$$\theta_{AA} = \theta_A + (1-\theta_A)\{1 - \exp[-5\theta_A/(1-\theta_A)]\} \quad \text{(A7)}$$

A further simplification gives the final result:

$$\theta_{AA} = 1 - (1-\theta_A)\exp[-5\theta_A/(1-\theta_A)] \quad \text{(A8)}$$

Manuscript received September 1, 1978; revision received August 8, and accepted August 30, 1979.

A Channel Flow Analysis for Porous Beds Moving Under High G Forces

An analysis is made of centrifugal flow of compacted porous beds through channels against high gas backpressure. One-dimensional compressible gas flow solutions are presented for concurrent and countercurrent solids/gas motion through the variable area channels. The physical process analyzed represents the flow through a newly developed centrifugal pump for feeding dry pulverized material against a pressure barrier. The objective of the analysis is to gain a basic theoretical understanding of this type of device. Good agreement is found between analytical predictions and test data obtained with an experimental pump feeding coal.

J. W. MEYER

Applied Mechanics Laboratory
Lockheed Palo Alto Research Laboratory
3251 Hanover Street
Palo Alto, California 94304

SCOPE

A new centrifugal pump has been recently developed for transporting dry pulverized material across a gas pressure barrier (Bonin et al., 1977). The experimental 1 ton/hr scale machine has successfully pumped coal from atmospheric pressure to delivery pressures as high as 2.8 MPa (400 lb/in.^{2} gauge). The heart of the pump is a high speed rotor that contains many converging radial channels or sprues. Pulverized material is transported into the eye of the rotor and centrifuged outward into the sprues. A compacted moving plug of porous material forms in the sprues and creates a seal against the high pressure gases. The sealing action is a combined effect of both the motion of the plug and its relatively low permeability.

The objective in the present paper is to develop a theoretical description of the basic operation of this new device, as well as a capability for predicting its performance. Specifically, the pump channel flow is analyzed, and solutions to the basic porous media flow problem are presented. A one-dimensional gas flow model is developed representing concurrent or countercurrent solids/gas motion through the variable area channels at high pressure ratios. Experimental data obtained in tests of the experimental machine pumping pulverized coal are presented, and comparisons with the theory are made. Attention here is focused exclusively on the rotor channel flow. Other aspects of the design of practical pump hardware are discussed elsewhere (Bonin et al., 1977; Lockheed, 1977*a*, *b*).

CONCLUSIONS AND SIGNIFICANCE

A theoretical approach has been developed to describe the porous media flow situation in the flow channels of a pulverized material pump. Theoretical model predictions based on uniform bed properties are in good agreement with operational experience with an experimental machine. The apparent permeability of the flowing material in the pump channels is found to be somewhat higher than measured in tests on static material plugs.

The theoretical model can be taken to be sufficiently validated to be useful in designing solids pumping machines to particular sets of requirements.

0001-1541-80-3684-0363-$01.25.

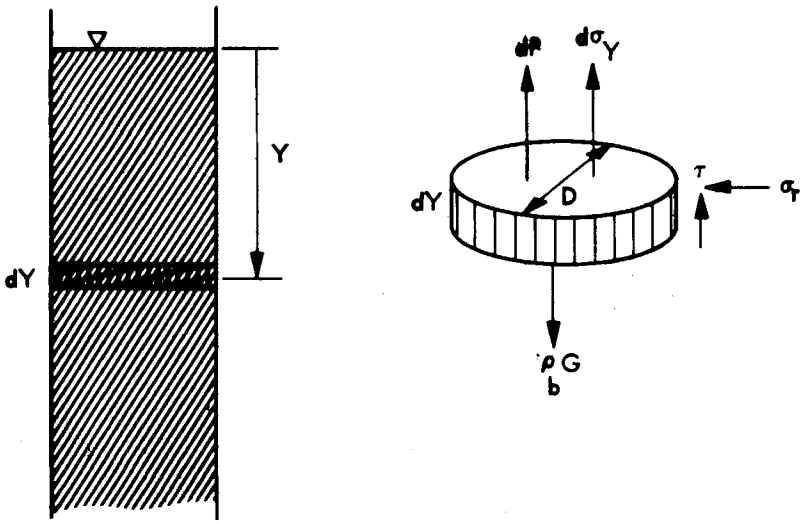

Fig. 1. Granular bed column stresses.

CHANNEL FLOW ANALYSIS

The flow of material in the pump rotor sprues has a basic similarity to the packed bed gravity transport of solids through standpipes or solid/fluid contacting columns that are widely used in the chemical industry. Stresses and friction forces in such columns have been investigated previously, using both one-dimensional (Delaplane, 1956; Brandt and Johnson, 1963) and two-dimensional models (Grossmann, 1975). This work has been drawn upon in the present stress analysis.

Consider a tall cylindrical or gently tapered bed of granular material in a radially oriented pump channel, such as illustrated by Figure 1. A control volume of bed material is subjected to centrifugal g forces which are opposed by a combination of gas pressure and granular material stresses. If we assume that the material flow velocity remains low, radial and coriolis accelerations can be neglected and the equilibrium force balance may be written as

$$\rho_b G - \frac{dp}{dy} - \frac{d\sigma_y}{dy} - \frac{4\tau}{D} = 0 \qquad (1)$$

After a development similar to that applied in the case of gravity standpipes (Delaplane, 1956; Brandt and Johnson, 1963), the stress ratios μ_1 and μ_2 are introduced:

$$\mu_1 = \frac{\tau}{\sigma_r} \; ; \quad \mu_2 = \frac{\sigma_r}{\sigma_y}$$

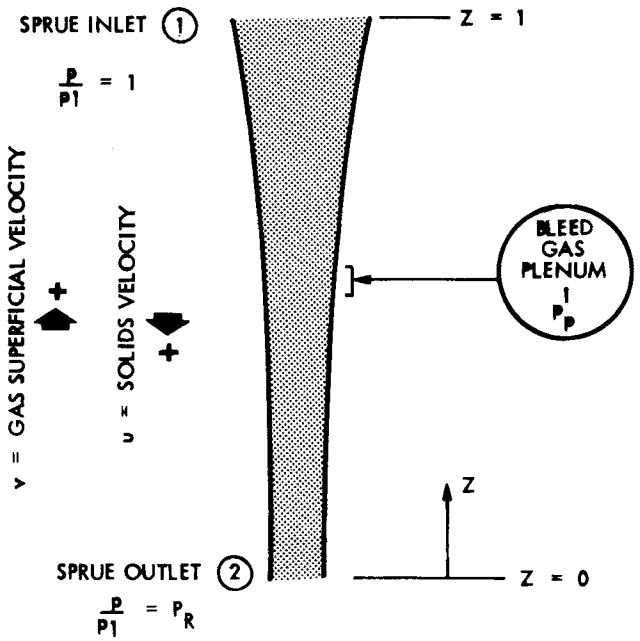

Fig. 2. Schematic of sprue flow situation modeled.

From these ratios, Equation (1) becomes

$$\rho_b G - \frac{dp}{dy} - \frac{d\sigma_y}{dy} - \frac{4\,\mu_1\,\mu_2\,\sigma_y}{D} = 0 \qquad (2)$$

If

$$\left(\rho_b G - \frac{dp}{dy}\right), \; \mu_1, \text{ and } \mu_2$$

are assumed constant, the solution of Equation (2) takes the form

$$\sigma_y = \frac{\left(\rho_b G - \frac{dp}{dy}\right) D}{4\,\mu_1\,\mu_2}\left[1 - \exp\left(\frac{-4\,\mu_1\,\mu_2\,y}{D}\right)\right] \qquad (3)$$

which, in the absence of the dp/dy term, is the well known Janssen's equation. According to Equation (3), the normal stress has an asymptotic value of

$$\sigma_y(\infty) = \frac{\left(\rho_b G - \frac{dp}{dy}\right) D}{4\,\mu_1\,\mu_2} \qquad (4)$$

for large y.

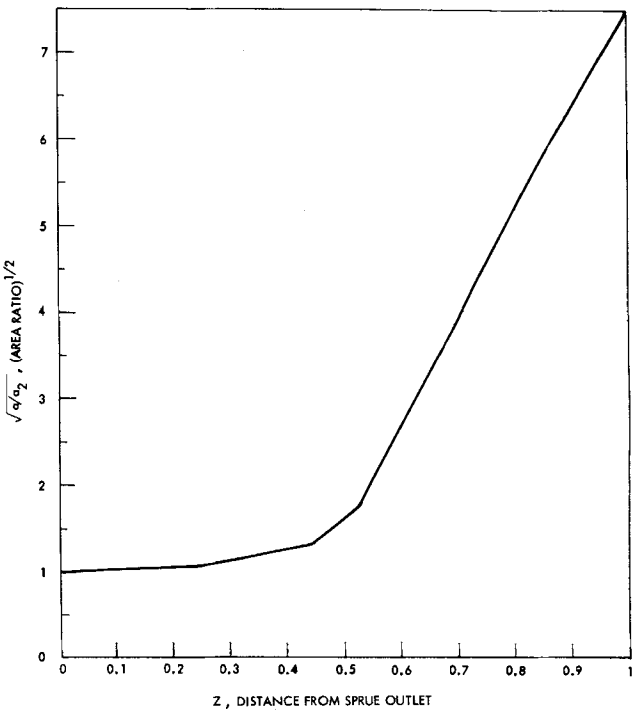

Fig. 3. Sprue shape profile for example calculation (area ratio)$^{\frac{1}{2}}$ vs. position.

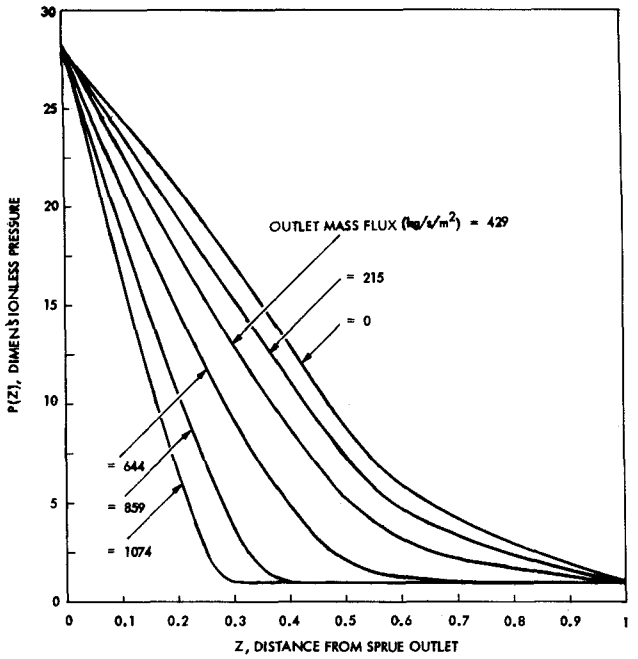

Fig. 4. Sprue gas pressure as function of position for the example. Sprue outlet solids mass flux as a parameter.

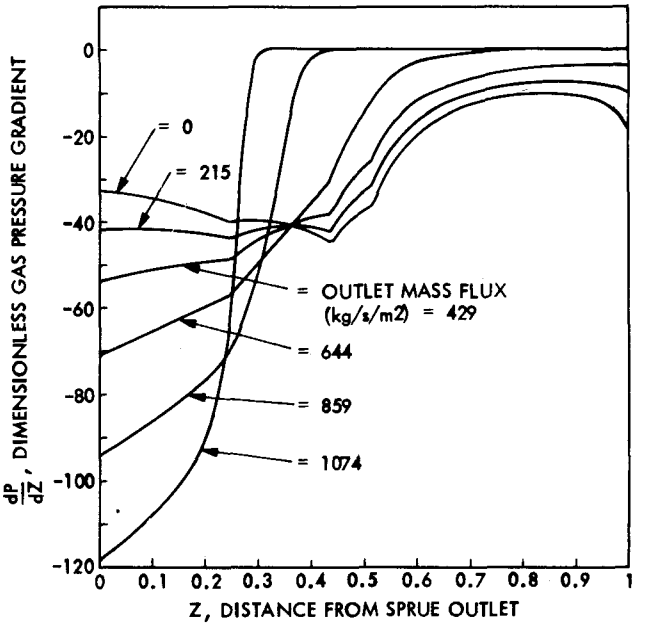

Fig. 5. Sprue gas pressure gradient as a function of position for the example. Sprue outlet mass flux as a parameter.

The coal feedstock used in the present experiments has a wall friction coefficient $\mu_1 \approx 0.5$; however, the exact value for the Janssen constant μ_2 was not determined. Jenike et al. (1972) recommend $\mu_2 = 0.4$ as representative of most materials. Using these data, $1/4\mu_1\mu_2 = 1.25$; in other words, the asymptotic stress $\sigma_y(\infty)$ represents the hydrostatic head only 1.25 diam below the bed surface. Wolf and Hohenleiten (1945) have published experimental column load data for pulverized coal which show an asymptotic head of about 2 diam.

Length-to-diameter ratios in the experimental rotor channels were quite large. The sprues tested were 21.3 cm in length with the channel span converging from 5 cm at the inlet to 1.3 cm at the midpoint, and then to from 0.6 to 0.9 cm at the outlet, depending on the particular set of hardware. Normally, most of the gas pressure drop takes place in the last 10 cm of the sprue, where the average diameter is only about 10% greater than the outlet. The conclusion to be drawn is that any buildup of σ_y in the sprues is very limited in magnitude, and, consequently, $d\sigma_y/dy$ is small throughout most of the flow channel, relative to the other terms in Equation (1). If we drop this term, the stress equation reduces to

$$\tau \approx \frac{D}{4}\left(\rho_b G - \frac{dp}{dy}\right) \tag{5}$$

This approximation can be expected to hold reasonably well everywhere except close to the inlet end of the sprue.

Evidently, over most of the sprue the force balance is quite simple. In the absence of a pressure gradient, the centrifugal body force and wall friction are in equilibrium. Imposing a gas

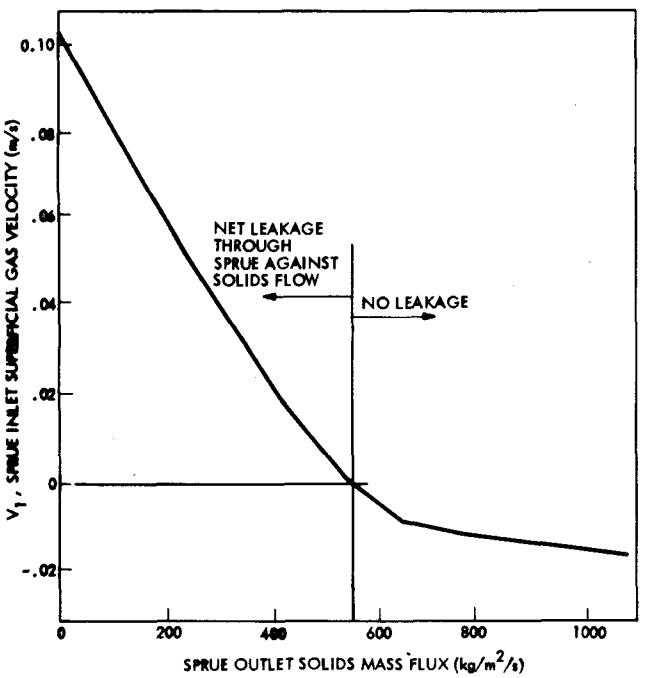

Fig. 6. Sprue inlet gas velocity as a function of outlet solids mass flux for the example.

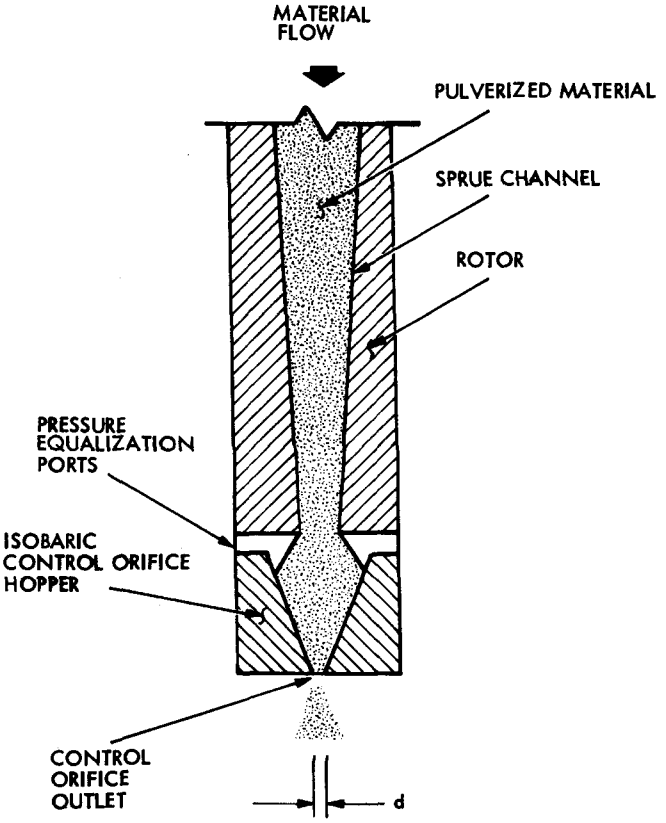

Fig. 7. Control orifice configuration.

pressure gradient merely reduces τ (and σ_y). This presumably has little effect until such time that $dp/dy = \rho_b G$ and the bed stresses completely disappear, that is, the material is fluidized. The introduction of the additional complications present in the actual pump rotor, namely, those of moderate variations of body force, pressure gradient and cross-sectional area along the channel, does not change this situation. Thus, the main requirement for pump channel design is just a proper matching between the body force distribution and the gas pressure gradient distribution in the channel. As long as the body force exceeds the pressure gradient so that the bed remains stressed to some degree, the pump will operate stably. This requirement is virtually local in character because of the short effective distances over which bed stresses can be transferred. Bed stresses could only be important insofar as they may influence the gas flow by changing bed porosity and permeability. Based on the experimental results to be discussed, this effect does not appear to have had a significant impact.

GAS FLOW SOLUTION

A one-dimensional porous media gas flow anaysis may be applied to the sprue flow. The theoretical model is formulated to handle gas bleed flows injected through the sprue walls into the medium, in addition to gas permeating upstream from the high pressure region. However, bleed flows were not used in the experiments discussed in the present paper. Using the nomenclature shown in Figure 2, where the origin is now fixed at the sprue outlet, we can apply the following equations to the problem. The Darcy equation is

$$v + \epsilon u = -\frac{k}{\mu}\frac{dp}{dz} \tag{6}$$

The gas and coal continuity equations are

$$-\rho q + \frac{\partial(\rho v a)}{\partial z} = -\epsilon\frac{\partial(\rho a)}{\partial t} \tag{7}$$

$$\rho_s u a = \dot{m} = \text{constant}$$

The gas equation of state under isothermal conditions is

$$\frac{p}{\rho} = \frac{p_1}{\rho_1} = \text{constant} \tag{8}$$

An unsteady form of the gas continuity equation is used here because the final equations are solved by means of a time asymptotic relaxation method. The bed parameters of bulk density, porosity and permeability, as well as the gas viscosity, are normally assumed to be constants in a given calculation. Introducing the following nondimensional variables of

$$A = \frac{a}{a_2}, \quad P = \frac{p}{p_1}, \quad Z = \frac{z}{L}$$

and defining

$$\beta \equiv -\frac{kp_1}{\mu L}$$

we get

$$v + \frac{\epsilon\dot{m}}{\rho_s a} = \beta\frac{dP}{dZ} \tag{9}$$

$$-\frac{\rho q}{a_2} + \frac{\partial(\rho v A)}{L\partial Z} = -\epsilon\frac{\partial(\rho A)}{\partial t} \tag{10}$$

$$\rho = \rho_1 P \tag{11}$$

By combining Equations (9), (10) and (11), a single, second-order differential equation for the pressure ratio is derived and is

$$-\epsilon AL\frac{\partial P}{\partial t} = \beta AP\frac{\partial^2 P}{\partial Z^2} + \beta A\left(\frac{\partial P}{\partial Z}\right)^2 + \left[\beta\left(\frac{dA}{dZ}\right)P - \frac{\epsilon\dot{m}}{\rho_s a_2}\right]\frac{\partial P}{\partial Z} - \frac{PqL}{a_2} \tag{12}$$

The boundary conditions are

$$P(0) = Pr, \quad P(1) = 1$$

The bleed gas is modeled by a simple incompressible orifice flow equation:

$$q_i = \frac{1}{\Delta Z_B^i}\,0.6\,a_B^i\left[\frac{2(p_P^i - p_1 P)}{\rho_P^i}\right]^{1/2}$$

$$\text{for} \quad Z_B^i \leq Z \leq Z_B^i + \Delta Z_B^i \tag{13}$$

The time asymptotic solution of Equations (12) and (13) constitutes the steady state sprue gas flow solution for a given problem. The computer code used to implement the solution uses a Z mesh of 129 points. An arbitrary (typically linear) pressure distribution is used as initial conditions and the equations are integrated forward in time until a steady state is reached. The final solution yields the pressure distribution along the sprue, the pressure gradient distribution along the sprue, the bleed gas flow rates (if any) and the gas leakage rate through the sprue.

Examples of results for a typical set of calculations without bleeds are given in Figures 3 through 6. The following set of constant parameters is assumed for the example: sprue length = 21.3 cm; solids bed permeability = 2.6×10^{-9} cm^2; solids bed density = 0.67 g/cm^3; solids bed porosity = 0.53; gas viscosity = 1.8×10^{-4} g/cm-s; sprue inlet gas pressure = 0.1 MPa (1 atm) and sprue outlet gas pressure = 2.8 MPa. Figure 3 gives the assumed sprue shape in terms of (area ratio)$^{1/2}$ as a function of position. Figures 4 and 5 give the calculated pressures and pressure gradients throughout the sprue as a function of position. The solids mass flux at the sprue outlet (that is, $\dot{m}/a_2$) is the parameter which distinguishes the several curves shown in each graph. Finally, Figure 6 gives the gas flow through the sprue in terms of the superficial gas velocity at the sprue inlet (Z = 1 position) as a function of solids mass flux. It may be noted that there is a particular value of mass flux, in the example it is about 550 kg/s/m^2, for which there is no gas flow whatsoever through the sprue ($v_1 = 0$). This is a desirable operating point to aim for in designing a pump.

It is clear from the plots in Figures 4 and 5 that the pressure distribution is sensitive to the mass flux, especially beyond the $v_1 = 0$ operating point. High mass flux tends to concentrate the pressure drop toward the outlet of the sprue. It is also found that variation of the medium permeability at constant mass flux produces similar looking families of pressure curves, and actually it is the ratio of mass flux to permeability that is the key factor. High mass flux/low permeability situations yield highly peaked pressure gradient distributions which are a poor match to the body force.

As discussed, for a pump to operate, the centrifugal body force in the medium must exceed the gas pressure gradient. In terms of the dimensionless variables, this requirement may be stated as:

$$\left|\frac{dP}{dZ}\right| < \left|\frac{\rho_b\, r\, \omega^2\, L}{p_1}\right| \tag{14}$$

The body force is linear in r (and Z) if the bed density in the sprue is constant.

In the experimental rotor, an essential component is a short end hopper or control orifice placed downstream of the sprue outlet as shown in Figure 7. This device acts to stabilize and to meter the material velocity through the sprue. Pressure equalization ports assure that there is no significant pressure difference across the control orifice itself. The flow of solids through the control orifice has been found to obey a Rausch type of gravity flow equation (Zenz, 1960), scaled by a $G^{\frac{1}{2}}$ factor to account for higher G forces; that is

$$\dot{m}_h = C\, d^{5/2}\, G^{1/2}$$

$$= C\, d^{5/2}\, (r)^{1/2}\, \omega \tag{15}$$

Thus, up to a certain limiting pressure, the end hopper runs full and the throughput is independent of delivery pressure, being only a function of rotor speed as given by Equation (15). Under conditions where the centrifugal force is insufficient according to Equation (14) criteria, and the maximum mass flow which can be delivered by the sprue is less than $\dot{m}_h$, the end

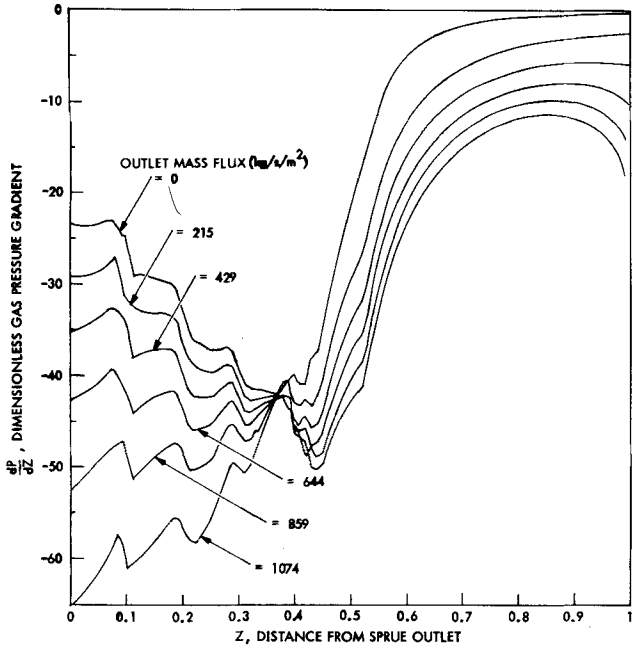

Fig. 8. Pressure gradient distributions obtained with gas bleeds through the sprue wall at Z = 0.1, 0.2, 0.3 and 0.4.

hopper would not run full. If this occurs, it has been found experimentally that the material plug in the sprue is unstable and can result in flow stoppages or blowbacks of high pressure gases into the rotor owing to a complete loss of the integrity of the sprue plug.

EFFECT OF GAS BLEEDS

One set of calculated results is presented in Figure 8 to generally illustrate the effect of gas bleeds distributed along the sprue walls. Four bleeds are assumed, all from a common plenum having a pressure of 3.62 MPa. All bleed orifices are assumed to be 1.9×10^{-7} m^2 in area, and a sprue outlet area of 4.9×10^{-4} m^2 is specified. Other data are identical to the previous example without bleeds.

Comparing Figure 8 and Figure 5, it can be seen that the effect of the gas injection is to reduce the pressure gradient in the region where gas is introduced, as would be expected.

MATERIAL PROPERTIES

The bulk material properties needed for theoretical calculations are the bulk density, porosity and permeability. Porosity is directly related to the bulk density by $\epsilon = (\rho_T - \rho_s)/\rho_T$. Therefore, only the bulk density and permeability at the state of compaction of the sprue material need to be estimated.

A laboratory apparatus was assembled to measure permeability of a compacted column of material. The schematic of the setup is shown in Figure 9. To measure permeability, the material sample is placed in the sample tube and compacted in a laboratory centrifuge. The sample tube is then placed in the Figure 9 apparatus, and the flow rate of gas permeating through the column is measured at a given pressure drop. The pressure drops are kept small so that the permeablity may be computed from an incompressible form of the Darcy equation. Specifically

$$k = \frac{Q_s \mu L_s}{A_s \Delta p_s}$$

The sample tubes are 2.2 cm in diameter, and a typical compacted column length was 5 to 6 cm.

Figure 10 shows permeability data obtained by the above procedure as a function of compacting G force in the centrifuge. The test materials are pulverized coal samples taken in conjunction with the coal pump experimental runs discussed later.

It is not altogether clear how to apply the Figure 10 data to the sprue flow situation. One approach would be assume the validity of Equation (4)

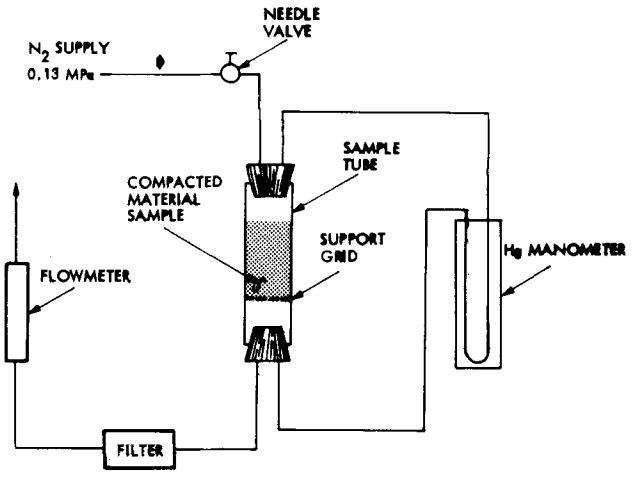

Fig. 9. Permeability test apparatus schematic.

$$\sigma_y = \frac{\left(\rho_s G - \frac{dp}{dy}\right) D}{4 \mu_1 \mu_2}$$

and to assume that k is directly related to σ_y. Thus, in the absence of a pressure gradient, $k = f(\rho_s G D)$. The average G force in the sprues in the experiments described in the following section was approximately 3 000 (g), which is three times higher than that which could be obtained in the lab centrifuge. On the other hand, over much of their length, the sprue diameters are two to four times smaller than the centrifuge tubes. Thus, using the $\rho_s GD$ scaling, the sprue material permeability would be expected to be similar to that near the 1 000 g compaction level in the lab tests. Finally, if the sprue pressure gradient represents a significant fraction of the sprue body force, a proportional reduction in the effective G force could be made.

EXPERIMENTAL HARDWARE

The coal pump hardware and test loop have been described elsewhere (Bonin et al., 1977) and will be only briefly reviewed here. The installation is shown schematically in Figure 11. The essential items are the atmospheric feed hopper, a feed tube for transporting fluidized material

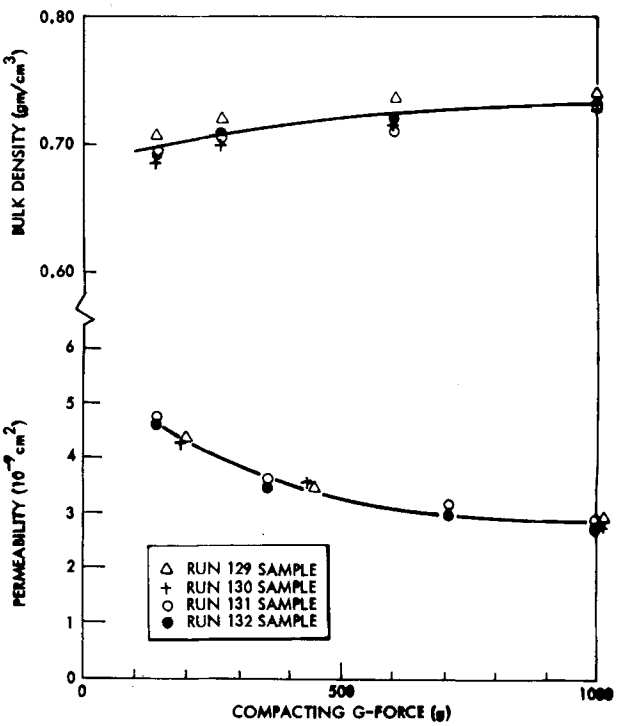

Fig. 10. Coal bulk density and permeability measured in lab centrifuge tests, 2.2 cm ID test tubes.

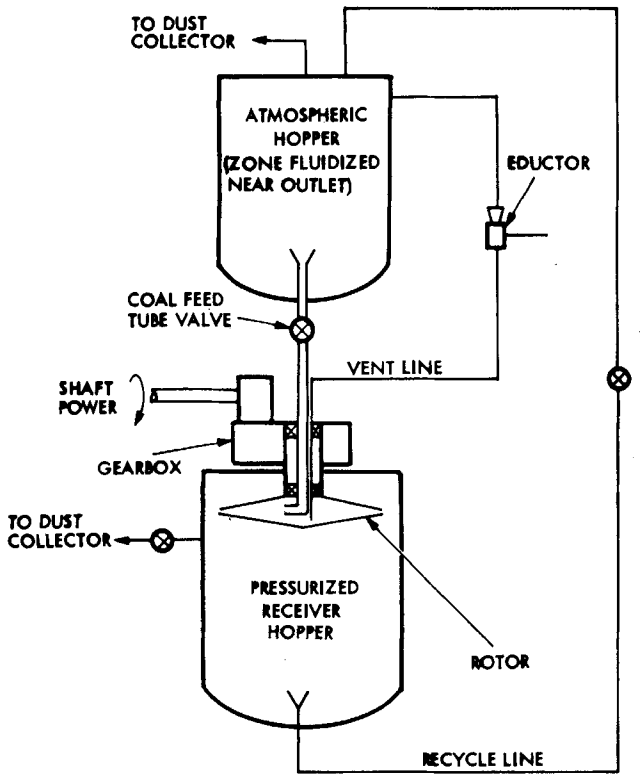

Fig. 11. Experimental test loop schematic.

into the eye of the rotor, the rotor and drive system, a vent line and an educator system for removing excess gases from the eye of the rotor and, finally, a high pressure receiver hopper. The feed hopper is zone fluidized near the feed tube inlet.

Tests of the coal pump at high delivery pressure are conducted on a batch basis. The pump cannot be started with a significant pressure difference across the sprue channel. Coal flow must be first initiated while the receiver hopper is at atmospheric pressure, and once the sprue plug is established, the hopper may be pressurized to the test level. To shut down, the procedure is reversed. Each of the vessels could hold approximately one-half ton of coal. However, when we allow for ullage and for time for pressurization and depressurization, steady state run times were normally about 5 to 10 min in duration.

The prototype rotor tested was 71.1 cm in diameter and contained twelve sprues which were replaceable parts so that shapes and cross-

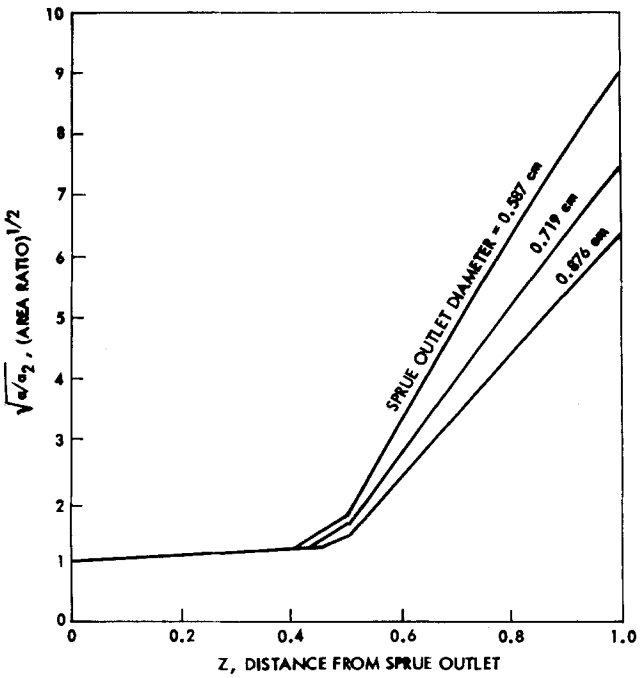

Fig. 13. Sprue shape profiles used in the experimental runs.

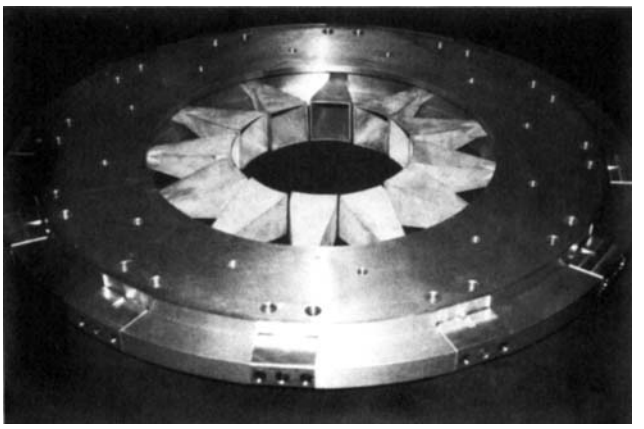

Fig. 12. Experimental rotor partial assembly.

sectional areas could be varied. A rotor subassembly is shown in Figure 12. The sprues are constructed in two approximately equal length sections, a cast funnel shape in conjunction with a machined cylinder. The wall angles in both sections are everywhere less than the material angle of slide, so that a uniform flow is obtained. In the experiments discussed in this paper, the funnel sections remained the same, and the sprue area profile changes were made only in the machined section.

EXPERIMENTAL RESULTS WITH PULVERIZED COAL

Complete validation of the computer analysis for the sprue flow is a difficult task. Definitive experimental data, for example, the sprue pressure distributions, cannot be obtained practically. Instead, indirect criteria were relied on, in this case gas backleakage through the sprues and maximum delivery pressure capability. The following pertinent data were obtained during experimental runs: coal throughput, delivery pressure, rotor speed, and rotor suction line flow rates. Throughputs are obtained by monitoring the weight change of the feed hopper, which is mounted on load cells.

Rotor suction line flow rates give a measure of the gas permeation flow rate through the sprue. In the experimental unit, excess gases are vented from the eye of the rotor through from one to three 0.46 cm ID channels. These vent lines are connected to a small eductor that discharges back into the feed hopper. Typically, the pressure at the eye of the rotor is kept at 0.07 to 0.09 MPa (−2 to −5 lb/in.^{2} gauge) to assure a constant flow into the rotor from the atmospheric pressure feed hopper. The minimum venting requirement is to remove the gas produced by compacting the coal from a fluid bed density, at which it enters the rotor, to the compacted bed density which it assumes in the sprues. This flow may be estimated from a gas mass balance on the rotor eye as follows. Coal enters the rotor eye at a fluidized density of approximately 400 kg/m^3 (72% porosity) and leaves at approximately 710 kg/m^3 (50% porosity). At a typical flow rate of 1 000 kg/hr, the minimum venting requirement is thus

$$Q_{min} = [1\ 000\ (0.72)/400] - [1\ 000\ (0.50)/710] = 1.1\ \text{m}^3/\text{hr}$$

Similarly, at the zero leakage point, the sprue gas velocity [v in Equation (6)] is zero, and all the gas entering through the feed pipe must be removed through the vent lines. In this case, $Q = 1.8$ m^3/hr.

The vent lines were calibrated so that flow rates could be computed from the pressure drop between the eye of the rotor and the eductor suction inlet. To properly correct for variations in gas density at the vent line inlet, the following pipe pressure drop equation was fitted to the line calibration data and was used to compute flows

$$Q = C_e(p_1 - p_e)^{1/2}(p_1)^{1/2}$$

It must be noted that the calibration was made using clean gas, whereas in coal pump operation a small loading of coal dust is entrained in the vent flows. The effect is believed to be small;

TABLE 1. COAL PUMP TEST DATA USED IN COMPUTER MODEL VALIDATION

Run No.	Sprue outlet diameter (cm)	Delivery pressure (MPa)	Rotor speed (rad/s)	Sprue outlet mass flux ($kg/s/m^2$)	Observed rotor vent flow (nm^3/hr)	Run duration at full pressure (min)	Comment
129	0.876	1.79	370	358	4.2	5	2 vent lines, pressure limit due to excessive gas backflow
130	0.587	2.23	376	805	Small	1	dP/dZ limiting behavior, — unstable/ blowback
131	0.719	2.79	376	537	5.6	6	3 vent lines, stable operation
132	0.719	2.86	376	537	6.5	7	3 vent lines, stable operation

however, strictly speaking, the apparent flow rates in tests must be treated as upper bounds.

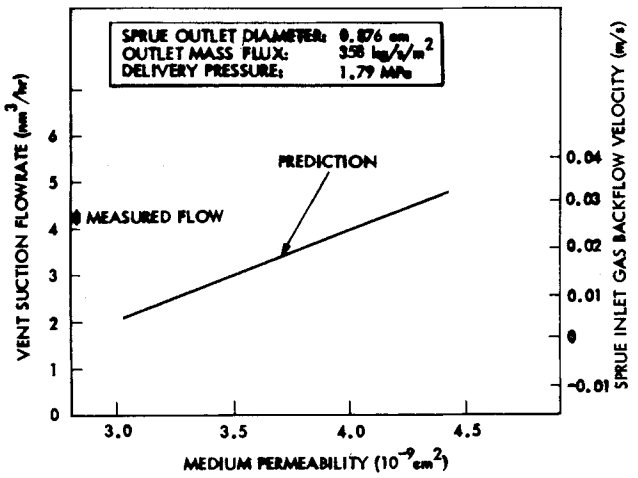

Fig. 14. Predicted gas backflow, as a function of bed permeability for run 129.

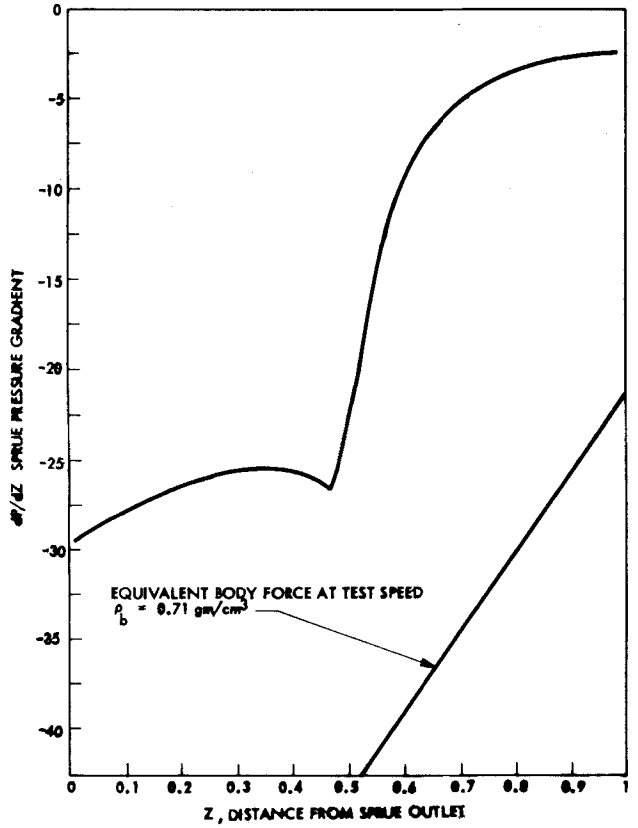

Fig. 15. Theoretical sprue pressure gradient distribution for run 129, $k = 3.6 \times 10^{-9}$ cm².

Experimental results obtained in a particular series of four successive coal pump runs, using the same well-characterized batch of coal, comprises the data set that will be used here to compare with theory. The feedstock was a Utah bituminous coal with a nominal 70% passing 200 mesh grind, and the pressurizing gas was nitrogen. All the runs were made at close to a 1 ton/hr rotor throughput and similar rotor speeds. Three sprue outlet sizes were tested. The outlet area of the largest size was 2.23 times that of the smallest, yielding a similar spread in the outlet velocity of the coal. Figure 13 shows the shape profiles of the sprues. Table 1 summarizes the experimental data for the series of tests. Estimates for the experimental error in the data are as follows: delivery pressure ±2%, mass flux ±5%, rotor speed ±1%, vent flow rate ±15%.

In run 129, the largest set of sprues was used (outlet diameter $D_2 = 0.878$ cm). At the observed throughput, the corresponding coal mass flux at the sprue outlet was 358 $kg/s/m^2$, and a delivery pressure of 1.79 MPa was reached. At this point, the total indicated rotor vent flow was 4.2 nm^3/hr. In run 130, a much smaller sprue set was installed ($D_2 = 0.587$ cm) which yielded an outlet mass flux of 805 $kg/s/m^2$. The rotor vent flow was then minimal, and the pressure limit was formed by the sprue pressure gradient exceeding the centrifugal force. As discussed, this has been found to yield unstable flow behavior and, in this case, a blowback.

In runs 131 and 132, the midsize sprue set was installed ($D_2 = 0.719$ cm), and a third rotor suction line was activated to increase

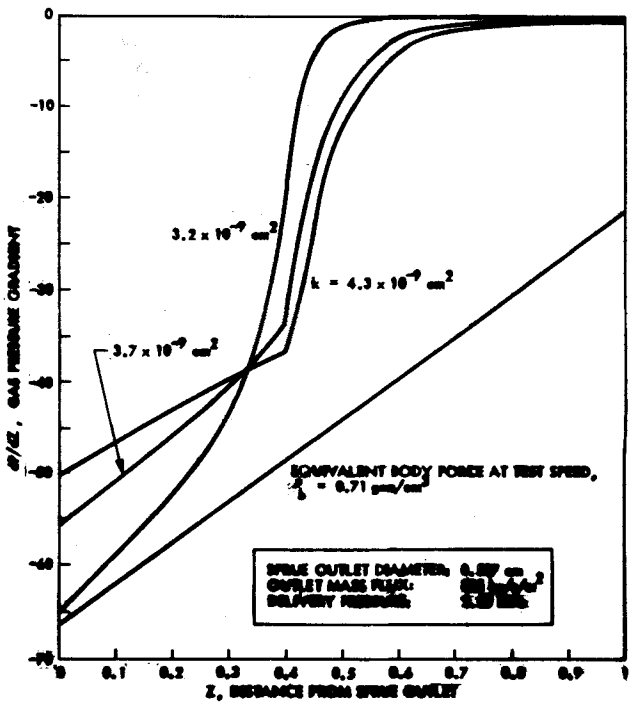

Fig. 16. Predictions for run 130 test. Pressure gradients for three values of bed permeability compared with body force.

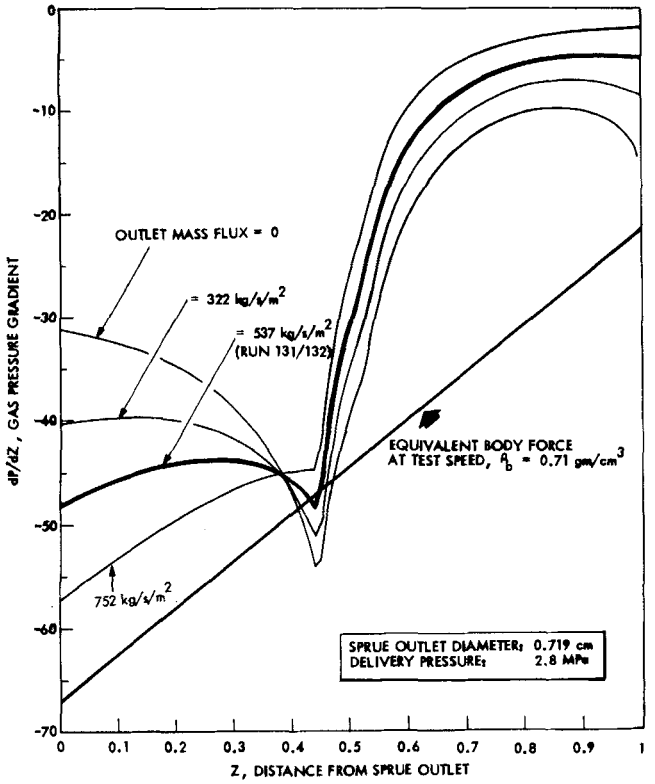

Fig. 17. Predicted gas pressure gradient distributions compared with body force, $k = 3.6 \times 10^{-9}$ cm², run 131/132 sprues.

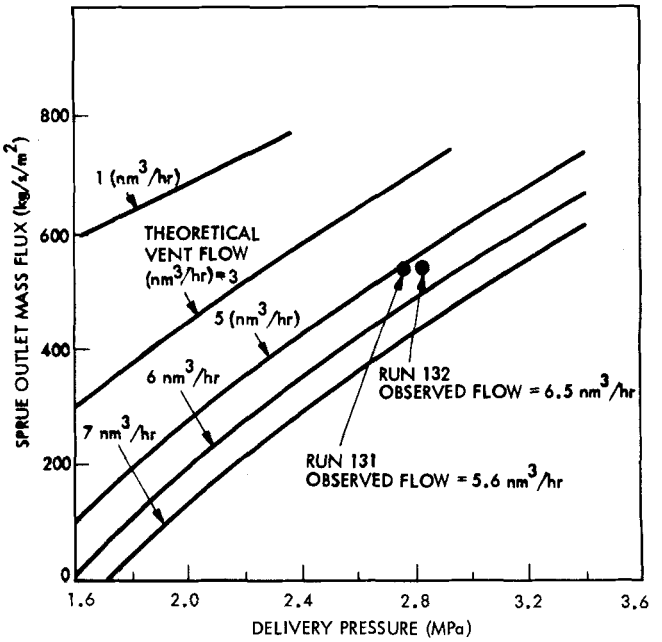

Fig. 18. Comparison of theoretical vent flows with observed flows in runs 131, 132. Predictions for $k = 3.6 \times 10^{-9}$ cm².

venting capacity. This enabled pressure levels of about 2.8 MPa to be reached.

COMPARISON WITH THE ONE-DIMENSIONAL THEORY

In this section, comparisons between the experimental data for runs 129 through 132 and predictions of the one-dimensional theory are made. It was found by trial and error that a single set of bed properties gives calculated results matching the data for all three sprue sizes.

To analyze runs 129 and 130, the theoetical model was exercised for the test pressures and mass fluxes with coal properties of $\rho_s = 0.71$ g/cm³, $\epsilon = 0.507$ and a range of permeabilities $k = 3.2 \times 10^{-9}$, 3.7×10^{-9} and 4.3×10^{-9} cm². This range spans what might represent conceivable states of compaction, based on the permeability tests on samples taken after each run (see Figure 10). The bed density value used is compatible with what is later shown to be the best fit permeability. A measurement of the true material density of the coal was made using a gas pycnometer, yielding $\rho_T = 1.44$ g/cm³ ± 1%. The porosity of $\epsilon = 0.507$ corresponds to this value with $\rho_s = 0.71$ g/cm³.

Figure 14 illustrates the results for the run 129 conditions. The graph shows the theoretical gas backflow through the sprues as a function of coal permeability. The measured vent flow for run 129 was 4.2 nm³/hr, which would correspond to the theoretical quantity if $k = 4.1 \times 10^{-9}$ cm². Since the measured vent flow must be interpreted as an upper limit, the apparent sprue medium permeability also constitutes an upper bound, that is, k (apparent) $< 4.1 \times 10^{-9}$ cm².

Figure 15 shows the theoretical pressure gradient distributions for the run 129 case, with $k = 3.6 \times 10^{-9}$ cm², which is later shown to be most representative permeability. The centrifugal body force in comparable units also is plotted, showing that it greatly exceeds the pressure gradient throughout the sprue.

Figure 16 illustrates the key theoretical results for the run 130 conditions. This figure gives a comparison of the centrifugal body force with the theoretical pressure gradient distributions obtained for the three k values. A blowback occurred in the test which is interpreted as dP/dZ having approached the body force too closely. According to the theory, the outlet dP/dZ would match the body force if $k \approx 3.1 \times 10^{-9}$ cm². This should be treated as a lower bound for the permeability in the sprue.

TABLE 2. THEORETICAL MODEL PREDICTIONS FOR $k = 3.6 \times 10^{-9}$ CM², $\rho_b = 0.71$ G/CM³, $\epsilon = 0.507$, COMPARED WITH TEST RESULTS

Run No.	Delivery pressure (MPa)	Sprue outlet mass flux (kg/s/m²)	Theoretical prediction	Experimental results
Run 129	1.79	358	Vent flow of 3.3 nm³/hr, ample body force	Vent flow of 4.2 nm³/hr, stable operation
Run 130	2.23	805	No gas backflow, outlet dP/dZ only 15% less than body force. Danger of blowback if slight decrease in permeability	No gas backflow, operated for short period then sudden blowback
Run 131	2.79	537	Body force 30% greater than dP/dZ at outlet but just below dP/dZ at $Z = 0.4$, 5.2 nm³/hr vent flow	Smooth runs with no blowback. Vent flows of 5.6 and 6.5 nm³/hr for runs 131, 132, respectively
Run 132	2.86	537	Same as above, 5.4 nm³/hr vent flow	

Therefore, it appears that if the theory and data are to be reasonably consistent for both sprue sizes, the actual sprue coal permeability must lie in the range

$$3.1 \times 10^{-9}\ \text{cm}^2 < k\ (\text{apparent}) < 4.1 \times 10^{-9}\ \text{cm}^2$$

The theoretical model was then exercised for the run 131 and 132 conditions (2.8 MPa delivery pressure), with the permeability in the middle of the apparent range $k = 3.6 \times 10^{-9}$ cm^2. These results are given in Figures 17 and 18. Figure 17 illustrates the gas pressure gradient distributions for a range of mass fluxes as compared to the body force in the run. For the test mass flux, the body force everywhere exceeds the calculated dP/dZ curve except for a very small region near Z = 0.4. The region is only about one half a diameter in length, so that it is plausible that a weak normal stress gradient could have forced the coal through this area. Figure 18 shows the comparison of theoretical and experimental gas backflow for the two runs. In this figure, the theoretical vent flow profiles are shown as a function of pressure and sprue mass flux. Measured vent flows in both runs are only slightly higher than the theoretical values.

A comparison of data and theoretical predictions for the runs for all three sprue sizes with $k = 3.6 \times 10^{-9}$ cm^2 are summarized in Table 2. Overall, the simple one-dimensional model calculations with uniform bed properties seem to be in good agreement with the observed test results. As can be seen, the high gas flow at low back-pressure for the large sprue is predicted by theory, the blowback with the small sprue is predicted and, finally, the successful operation and leakage rates at 2.8 MPa, using the optimal sprues, is predicted reasonably well.

It should be noted that the sprue material permeability value that provides a good fit to the data, $k = 3.6 \times 10^{-9}$ cm^2, is somewhat higher than might be expected based on the lab centrifuge measurements. The reduction in compaction stress due to the partial support of the sprue material by the gas pressure gradient does not appear to be nearly enough to account for the increase. This is especially clear in run 129 which utilized the largest diameter sprues and the largest excess of body force over the pressure term. Relatively speaking, the compaction of the coal should have been the greatest and the apparent permeability the least, in this case. However, no such effect can be discerned in the data. It may be speculated that the high apparent permeability in mainly due to the fact that the lab tests were performed on stationary compacted plugs, whereas the material remains in motion in the coal pump sprues. The dilatation associated with the motion reduces the compaction density to less than that obtained in a static condition and washes out the effect of stress level variations.

ACKNOWLEDGMENT

This research was supported by the U.S. Department of Energy under Contract No. E(49-18)-1792 and program manager R. R. Fleischbein. The author also wishes to acknowledge the contribution of J. J. Kohfeld who ably programmed the computer code.

NOTATION

A = area ratio a/a_2
A_s = sample column cross-sectional area
a = channel area
a_B^i = i^{th} bleed gas orifice area
C = empirical constant
C_e = suction line constant, 0.97 nm^3/hr/MPa$^{1/2}$
d = control orifice outlet diameter
D = channel diameter
G = $r\omega^2$ centrifugal acceleration
k = bed permeability
L = sprue length
L_s = sample column length
$\dot{m}$ = solids mass flow rate
$\dot{m}_h$ = mass flow rate defined by Equation (15)
P = pressure ratio p/p_1
p = gas pressure
p_P^i = plenum pressure of bleed gas
Δp_s = pressure drop across sample column
Pr = total pressure ratio across sprue
Q = rotor vent gas flow rate
Q_s = volume flow rate through sample
q = bleed volume flow rate per unit sprue length
q_i = volumetric flow per unit sprue length
r = distance from rotational axis
t = time
u = solids radial velocity
v = gas superficial radial velocity
y = depth below bed surface
z = distance from sprue outlet
Z = z/L
Z_B^i = bleed port location
ΔZ_B^i = length over which bleed gas injection takes place

Greek Letters

β = $-\ k\ p_1/\mu L$
ϵ = bed porosity
ρ = gas density
ρ_b = total bed density
ρ_s = bed solids density
ρ_T = true material density
ρ_P^i = density of bleed gas
μ = gas viscosity
μ_1, μ_2 = Janssen stress ratios
τ = wall shear stress
σ_r = material stress normal to wall
σ_y = average material stress in y direction

Subscripts

1 = sprue inlet
2 = sprue outlet
e = eductor inlet

LITERATURE CITED

Bonin, J. H., D. E. Cantey, A. D. Daniel and J. W. Meyer, "Development of Dry Coal Feeders," *Proceedings of the Conference on Coal Feed Systems*, June 21-23, 1977, JPL Publication 77-55, Jet Propulsion Lab., pp. 195-239 (1977).

Brandt, H. L., and B. M. Johnson, "Forces in a Moving Bed of Particulate Solids With Interstitial Fluid Flow," *AIChE J.*, **9**, No. 6, 771-777 (Nov., 1963).

Delaplane, J. W., "Forces Acting in Flowing Beds of Solids," *ibid.*, **2**, No. 1, 127-138 (Mar., 1956).

Grossman, Gershon, "Stresses and Friction Forces in Moving Packed Beds," *ibid.*, **21**, No. 4, 720-730 (July, 1975).

Jenike, A. W., J. R. Johanson and J. W. Carson, "Bin Loads III, Mass Flow Bins," paper presented at the Second Symposium on Storage and Flow of Solids, Chicago, Ill. (Sept. 17-20, 1972).

Lockheed, *Coal Feeder Development Program Phase II Report*, FE-1792-34, Dist. Category UC-906, Lockheed Missiles & Space Company, Inc., Sunnyvale, Calif. (July, 1977*a*).

Lockheed, *Coal Feeder Development Program, Oct-Dec Quarterly Report 1977*, FE-1792-40, Dist. Category UC-906, Lockheed Missiles & Space Company, Inc., Sunnyvale, Calif. (Dec. 1977*b*).

Wolf, E. F., and H. L. Hohenleiten, "Experimental Study of the Flow of Coal in Chutes at Riverside Generation Station," *ASME Trans.*, **67**, 585-599 (1945).

Zenz, F. A., and D. F. Othmar, *Fluidization and Fluid Particle Systems*, Reinhold, New York (1960).

Manuscript received June 4, revision received October 1, and accepted October 11, 1979.